Pure Appl. Chem., Vol. 81, No. 8, pp. 1511–1522, 2009.
doi:10.1351/PAC-CON-08-08-34

Spectroscopy of a single Sb_2Se_3 nanorod*

Kien Wen Sun[1,‡], Cheng-Hang Yang[1], Ting-Yu Ko[1], Hao-Wei Chang[2], and Chen-Wei Liu[2]

[1]Department of Applied Chemistry and Institute of Molecular Science, National Chiao Tung University, Hsinchu 30010, Taiwan; [2]Department of Chemistry, National Dong Hwa University, Hualien 97401, Taiwan

Abstract: In this paper, we present solvothermal methods to chemically synthesize Sb_2Se_3 nanorods using dialkyl diselenophosphate (dsep) complexes of antimony. Energy-dispersive X-ray analysis shows the products are phase pure. We have also studied the Raman and photoluminescence spectroscopy of a single Sb_2Se_3 nanorod with an average size of 60 nm in diameter and a length less than 1 μm. Techniques have been devised to immobilize and allocate a single nano-object on an electron beam (E-beam) patterned smart substrate with metallic coordination markers. This also overcomes the limitation of spatial resolution of conventional optical techniques (~1 μm) to perform optical spectroscopy on an individual nano-object less than 100 nm in size. Raman spectroscopy reveals that Sb_2Se_3 nanorods synthesized at a lower temperature contain a small amount of Sb_2Se_3. The broad linewidth observed in luminescence spectra from a single rod is attributed to the increasing number of surface defects, impurities, and dangle bonds attached on the surface as the nanoparticle size reduced to nanometer scale.

Keywords: nanorods; Raman; photoluminescence; electron beam lithography; solvothermal.

INTRODUCTION

In recent years, V_2VI_3-type semiconductors, which have a bandgap energy range from 2.2 (Sb_2Se_3, as an example) to 0.21 eV (such as Bi_2Te_3) have been widely studied. In particular, the antimony triselenide (Sb_2Se_3), which is a layer-structured semiconductor of an orthorhombic crystal structure, has attracted considerable attention due to its switching effects [1] and good photovoltaic and good thermoelectric properties [2,3]. Thin polycrystalline films of Sb_2Se_3 semiconductors are commonly used as absorber films for the fabrication of cost-effective solar cells and Hall effect devices [4]. The high thermoelectric power of these films provides scope for possible applications in optical, thermoelectric cooling, and power conversion devices [5]. Rosi et al. found the Peltier effect in Sb_2Se_3 and utilized this effect for cooling [6]. Platakis et al. reported threshold and memory switching phenomena on the materials of Sb_2Se_3 [1]. It has also been used in photoelectronics in the infrared region [7,8]. Due to these useful properties, Sb_2Se_3 has been attracting great research attention.

Over the last decade, various methods have been demonstrated for synthesis and characterization of 1D nanostructure V-VI group semiconductor compounds. These 1D nanostructures can be used as building blocks for many novel functional materials and devices. The synthesis of Sb_2Se_3 nanorods has

*Paper based on a presentation at the 8th Conference on Solid State Chemistry, 6–11 July 2008, Bratislava, Slovakia. Other presentations are published in this issue, pp. 1345–1534.

‡Corresponding author; Tel.: 886 3 571 2121, ext. 56581; Fax: 886 3 572 3764; E-mail: kwsun@mail.nctu.edu.tw

been demonstrated using a hydrothermal reduction route [9]. It was found that hydrazine as both the reducing agent and the coordinator was crucial for the formation of the rod-like morphologies. The solvothermal synthesis of crystalline Sb_2Se_3 nanowires with a high aspect ratio in diethylene glycol media was reported by Wang et al. [10]. Nanoribbons with diameters in the range of 25–100 nm and length of 10s of micrometers have been synthesized via a simple hydrothermal process [11]. More recently, Zhang et al. [12] reported the synthesis of Sb_2Se_3 hollow nanospheres prepared by solvothermal treatment of $SbCl_3$ and selenium powder in the presence of cetyl trimethylammonium bromide (CTAB). The control synthesis of novel Sb_2Se_3 and Sb_2Se_3 nanostructures with a sheaf-like and dumbbell morphology has been demonstrated under hydrothermal treatment in the presence of poly-(vinyl pyrrolidone) (PVP) polymer by Chen and coworkers [13]. These nanomaterials may eventually lead to technological applications in the manufacture of optoelectronic nanodevices due to their remarkable electronic, optical, catalytic, and mechanic properties.

In the earlier works [14–20], the preparation of Sb_2Se_3 nanomaterials all started with reactions between metal precursors (antimony chloride, bismuth chloride, or bismuth nitrate) and selenide precursors (selenide powder, NaHSe, Na_2SeSO_3, or H_2SeO_3). In this report, we demonstrate the synthesis of the dialkyl diselenophosphate (dsep) and the metal precursor $Sb(C_2H_3O_2)_3$ and the fabrication of nanocrystalline Sb_2Se_3 from the single-source precursor $Sb[Se_2P(O^iPr)_2]_3$ at different temperatures via solvothemal methods. To our knowledge, the synthesis of nanocrystals by a single-source precursor method has not been reported. The potential advantage includes ease of separation of the nanocrystalline material and better control over the size and shape, as fewer parameters need to be manipulated. The optical properties of the single Sb_2Se_3 nanostructure were measured at room temperature by dispersion, immobilization, and allocation of a single nanorod on silicon substrates patterned with coordination markers using E-beam lithography techniques.

EXPERIMENTAL

Synthesis of Sb_2Se_3 nanorods

In 1968, Zingaro studied the reaction of phosphorus pentaselenide (P_2Se_5) with a number of alcohols (absolute ethanol, propan-2-ol, butan-2-ol) and synthesized dialkyl dsep and potassium complexes [21]. Our synthesis of the $Sb[Se_2P(O^iPr)_2]_3$ precursor was adapted from a modified procedure that Zingaro et al. [22] used to prepare $Sb[Se_2P(OEt)_2]_3$.

A suspension of $NH_4[Se_2P(O^iPr)_2]_3$ (1.00 g, 3.067 mmol) in dichloromethane (40 ml) was added to $Sb(OAc)_3$ (0.306 g, 1.025 mmol), and the resulting mixture was stirred for 4 h under N_2 then filtered through Celite under a N_2. The yellow filtrate was collected and evaporated to dryness using a rotary evaporator under reduced pressure. The solid residue was dissolved in hexane (20 ml), filtered through Celite, and evaporated to dryness. The resultant yellow powder $Sb[Se_2P(O^iPr)_2]_3$ was crystallized from dichloromethane layered with hexane to furnish single crystals suitable for X-ray crystallography.

$Sb[Se_2P(O^iPr)_2]_3$. $Sb[Se_2P(O^iPr)_2]_3$ (0.8 g, 0.767 mmol) was added to methanol (20 ml) and heated in a Teflon-coated stainless steel autoclave at either 100 or 150 °C for 12 h. The black residue, obtained upon cooling to room temperature, was washed with methanol (3 × 1 ml) and dried at 70 °C for 5 h. Powder X-ray diffraction (XRD) and energy-dispersive spectrometry (EDS) revealed that the solid was Sb_2Se_3. Details on the synthesis of the precursor and the Sb_2Se_3 nanorods have been published elsewhere [23,24].

Spectroscopy of a single nanorod

We first diluted the 0.001 g of Sb_2Se_3 nanorod powder fabricated at 100 °C in 10 ml DI water and ethanol mixture. The solution was then placed in an ultrasonic bath operated at a vibration frequency of 185 KHz for 30 min to prevent formation of nanorod clusters. Due to the acoustic cavitation effect

[25], the ultrasonic wave heated up the water and broke the water molecules into H^+ and OH^- ions. The OH^- ions attached to the nanorod surface and induced a Coulomb repulsion force between the nanostructures. Therefore, clustering of nanorods was avoided. A test drop of the solution was placed on a bare Si wafer, and after solution had dried out, scanning electron microscope (SEM) images were taken to examine the clustering of nanorods. The concentration of solution was continuously adjusted until nanorods were well dispersed on the template. The preparation of patterned smart substrates is explained as follows.

We designed and fabricated a coordination system on Si templates for labeling a dispersed single nanorod. The templates used in experiments were commercially available 4-inch silicon wafers with (001) crystal orientation and n-type background doping. The Si wafer was first diced into 2 × 2 cm chips. As shown in Fig. 1, a pattern of 2D array cross-finger type metal wires with a linewidth of 500 nm, a pitch of 1 μm, and a length of 50 μm was defined on the Si chip using E-beam lithography within an area of 1 mm^2. On the right- and left-hand sides of the patterned area, we defined a series of rectangular and square position markers (with dimensions of 10 × 30 μm and 10 × 10 μm, respectively), so the coordinates could be easily counted under an optical microscope. The pitch and metal linewidth were determined according to the laser spot size (~1 μm) and optical resolution of our confocal microscope (~300 nm) at the excitation wavelength of 532 nm. Schematics of the lithography processes are shown in Fig. 2. A drop of well-diluted Sb_2Se_3 nanorod solution was placed on the patterned template as shown in Fig. 3.

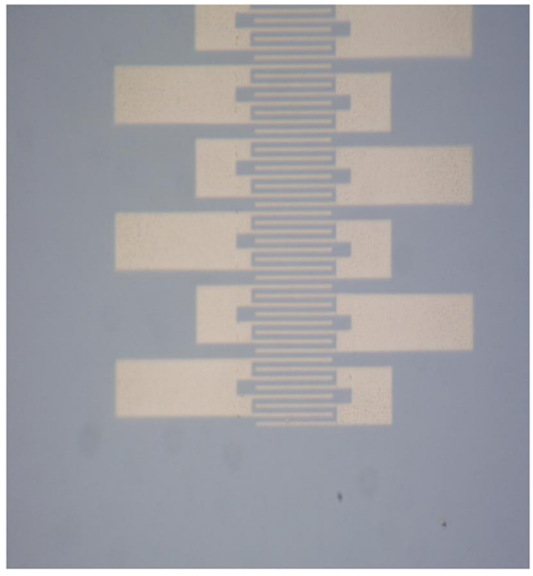

Fig. 1 Optical image of the cross-finger-type coordination markers.

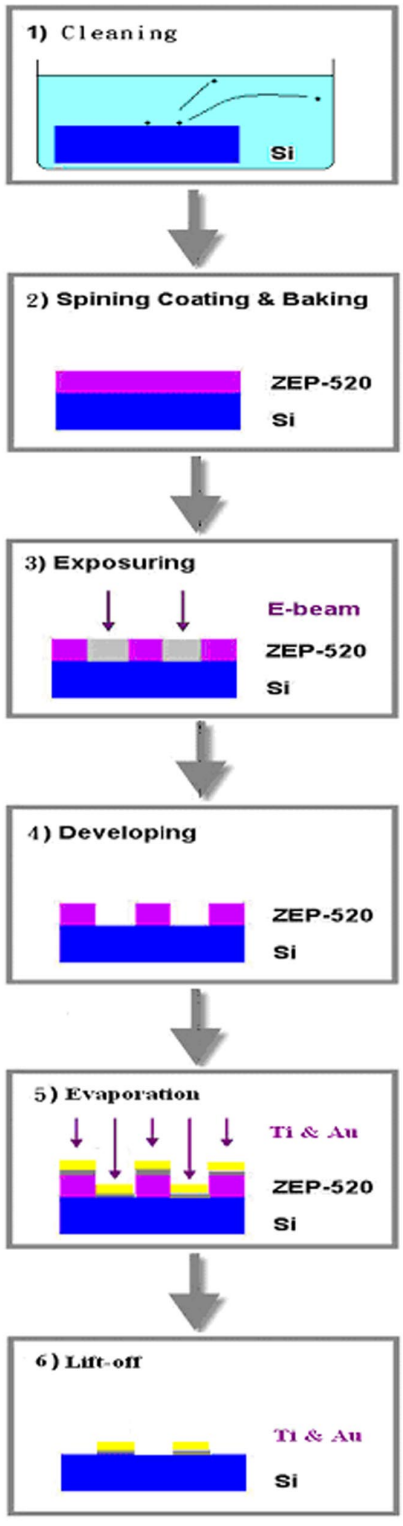

Fig. 2 Flow chart of the photolithography processes.

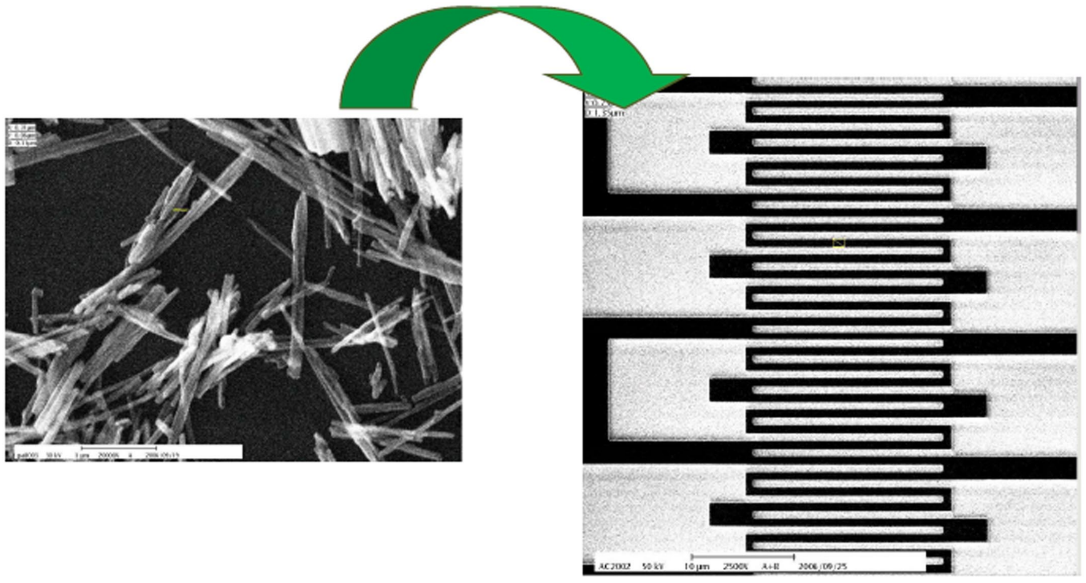

Fig. 3 Well-dispersed Sb_2Se_3 nanorods were spread on the patterned template.

After the sample had dried out, the surface was scanned by SEM to allocate a single nanorod. Figure 4 shows the SEM scanning results of a single nanorod with a diameter of 70 nm and a length of 0.5 μm nearby a coordination marker. Most importantly, from the SEM image, we were able to ensure that there was no other nanorod within the laser focus spot but the selected target before the optical measurements. After the targets were allocated, their corresponding coordinates were assigned. Figure 5 shows the optical image of patterned substrate. The dimension of coordination markers was properly designed so they could still be clearly seen under the optical microscope. The entire template was moved via an X-Y stepping motor to the given coordinate to position targets under the laser spot,

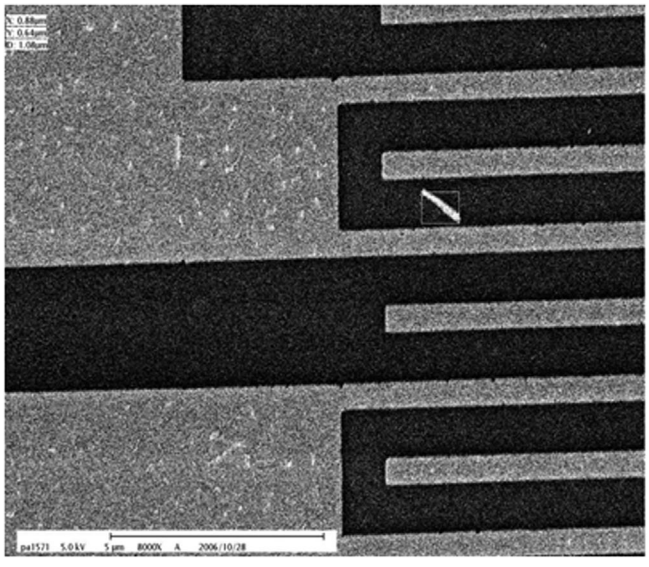

Fig. 4 SEM image of a single Sb_2Se_3 nanorod immobilized on the patterned substrate.

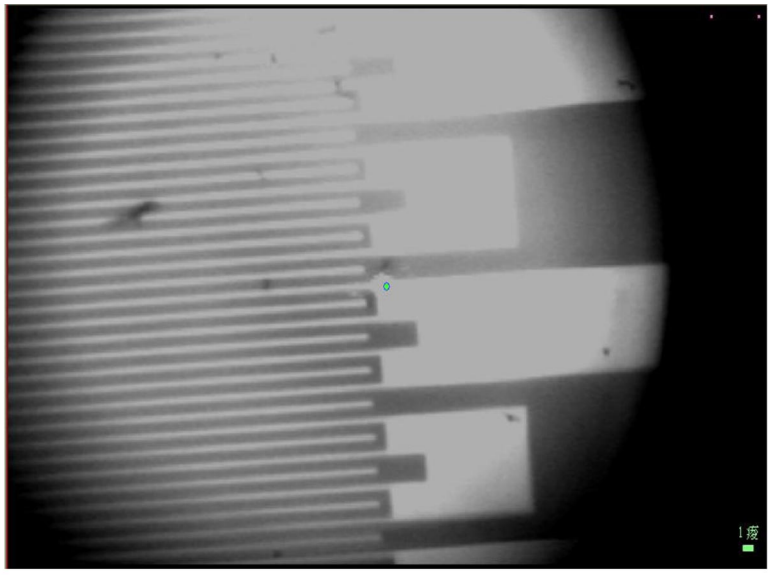

Fig. 5 Optical image of the patterned substrate with immobilized Sb_2Se_3 nanorods.

while the optical image of substrate was simultaneously monitored on a TV screen. The optical signals were collected at room temperature through the microscope objective and were analyzed by a 0.32-m spectrometer equipped with a liquid nitrogen-cooled charge-coupled device (CCD) detector at the excitation wavelength of 532 nm. The optical signal was further optimized by adjusting the focal plane position along the *z*-axis via the piezo-driven objective lens. The acquired spectra were averaged to achieve a good signal-to-noise ratio.

RESULTS AND DISCUSSION

SEM images of fabricated nanorod clusters and a single nanorod are shown in Figs. 6 and 7. Sb_2Se_3 nanorods made at 100 °C have an average diameter of 30–50 nm and an average length of 2–3 μm (as shown in Fig. 6a). However, for the rods made at 150 °C, the SEM images show a slightly larger diameter of 70–90 nm and an average length of 3–5 μm (as shown in Fig. 6b). Figure 8 shows the XRD pattern of nanorods. Synthesis at both temperatures can be indexed with the orthorhombic crystal system with the space group Pnma, and the cell parameters a = 11.63 Å, b = 3.99 Å, and c = 11.78 Å were able to meet the standard values in the Joint Committee on Powder Diffraction Standards (JCPDS) 15-0861 documents. EDS analysis, as shown in Fig. 9, indicates that the Sb/Se atomic ratio is 39.9:60.0 (close to 2:3), giving the nanorod a possible composition of Sb_2Se_3. In short, the intrinsically anisotropic, layered crystalline structure of Sb_2Se_3 plays an important role in favoring the crystal growth along the formation of 1D nanostructures. Furthermore, the precursor fragments produced from the thermal decomposition of the single-source precursor may contribute to favor the formation of 1D nanostructures further.

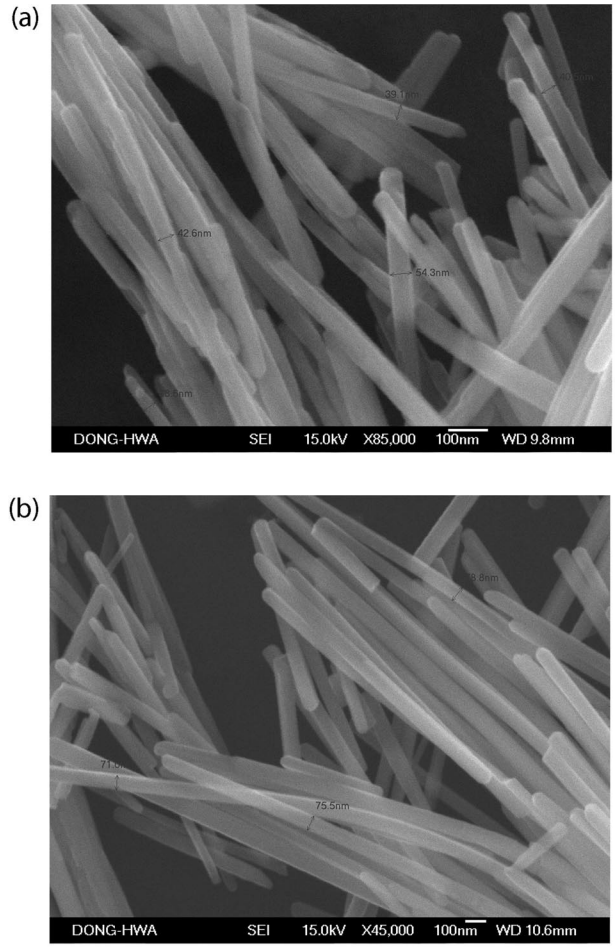

Fig. 6 SEM images of the Sb_2Se_3 nanorod clusters fabricated at (a) 100 °C, (b) 150 °C.

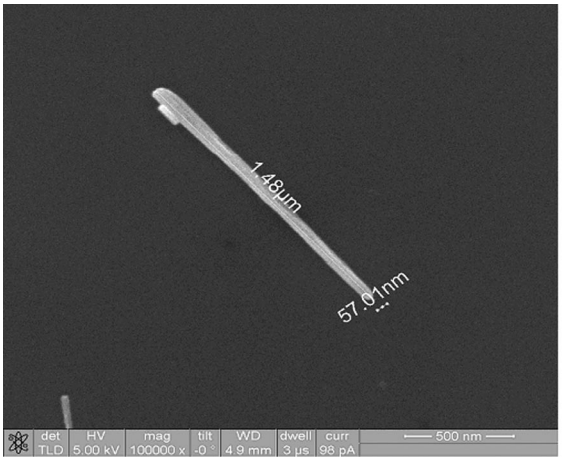

Fig. 7 SEM image of a single Sb_2Se_3 nanorod with a length of ~1.5 μm and a diameter of ~60 nm.

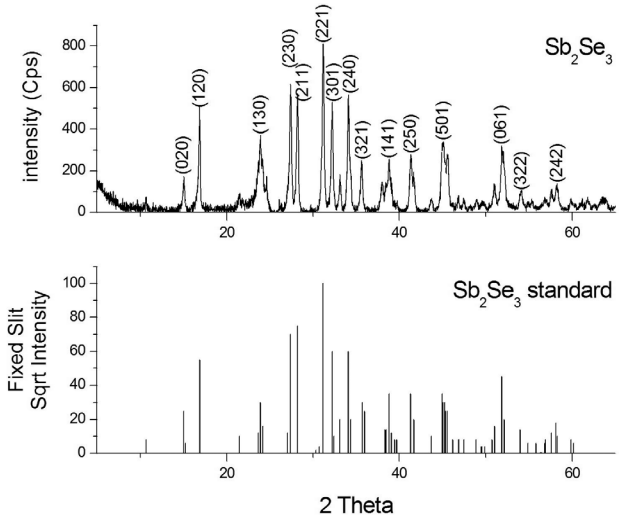

Fig. 8 XRD pattern of the Sb_2Se_3 nanorods. (Sb_2Se_3 standard: JCPDS 15-0861).

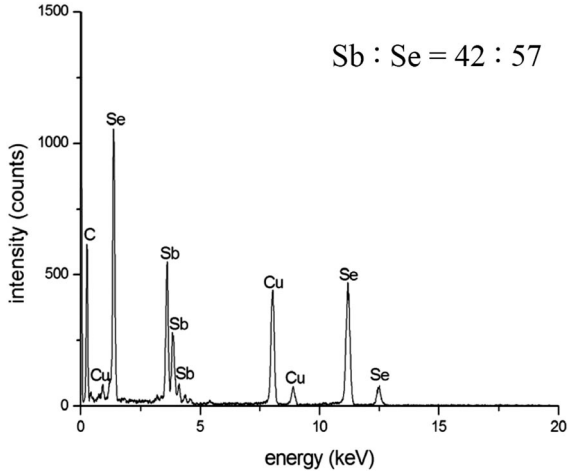

Fig. 9 EDS result that indicates that the nanorods are composed of Sb_2Se_3.

The UV–vis light absorption spectrum of nanorod clusters in the range of 200–1200 nm, as shown in Fig. 10a, has a maximum of 688 nm. The absorption coefficient α is determined by the following equation:

$$\alpha = \frac{[B(E - E_g)^n]}{E}$$

where $E = \hbar\omega$, B is determined by the effective mass of valance band and conduction band and $n = 1/2$ for the direct band material. Figure 10b shows the absorption coefficient as a function of energy. The extrapolation of this curve gives the energy of direct bandgap (E_g) at 1.17 eV. The estimated bandgap energy of nanorods is comparable to the value (1.13 eV) reported in [13], which is also not affected by the quantum confinement effect at their present dimension. It can be due to the lower Bohr's radius for this material.

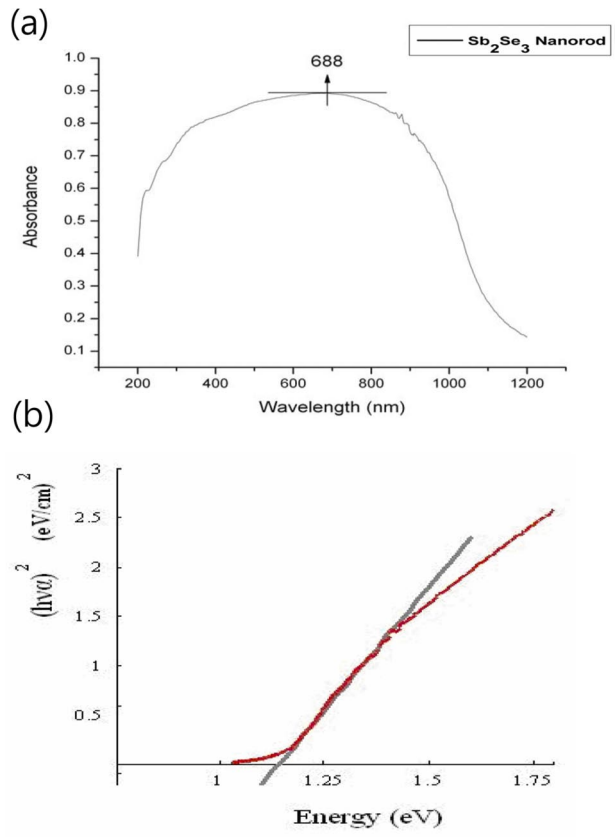

Fig. 10 (a) The UV–vis light absorption spectrum (b) the calculated absorption coefficient as a function of energy.

In Fig. 11a, photoluminescence spectrum of more than 200 nm in full width at half maximum (FWHM) and centered at 710 nm was observed from the nanorod powder. However, for the single nanorod, a narrower PL emission centered at about 700 nm with an FWHM of 125 nm was observed at an excitation wavelength of 532 nm as shown in Fig. 11b. The broader linewidth of nanorod powder is due to the size distribution of rods. The exponentially decaying tail near 560 nm in Fig. 10 is due to the Si Raman signal from substrate. The features on this broad emission can be fitted with a single Lorentzian peak centered at 695 nm, although similar PL results were reported by Ma et al. [26] on wire-like microcrystalline Sb_2Se_3 powder excited with UV laser light. Their experimental results indicated a PL peak at 707 nm but with a much narrower FWHM of only 25 nm. The broad emission peaks observed in our experiment originate from the increasing number of surface defects, impurities, and dangle bonds attached to the surface as the dimensions of the nanostructures were reduced from micrometer to nanometer scale.

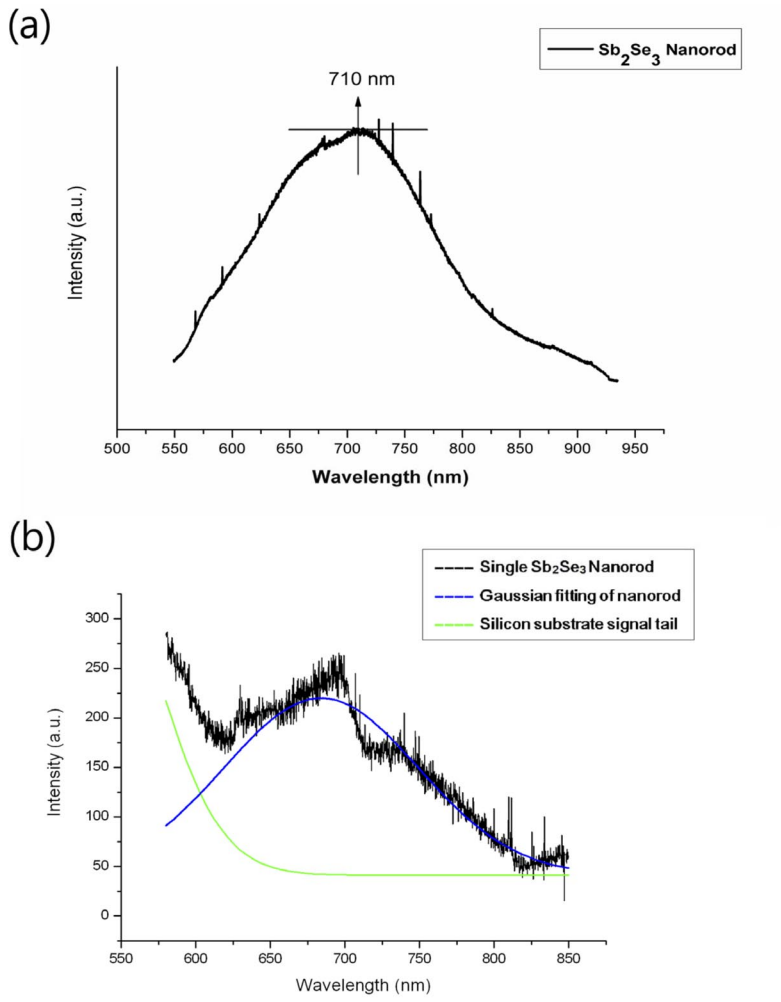

Fig. 11 Photoluminescence spectra of (a) Sb_2Se_3 nanorod clusters and (b) a single Sb_2Se_3 nanorod.

In the Raman measurements, we have identified four peaks at 147, 187.5, 229.5, and 252 cm^{-1} from the single Sb_2Se_3 nanorod fabricated at temperature of 100 °C (as shown in Fig. 12a). Our Raman measurements agree well with the earlier results [9,12,26] of the Sb_2Se_3 nanorods, nanospheres, and nanowires clusters. It appears that the shape of the nanostructures does not affect the Raman spectra. The main peak at 187.5 cm^{-1} corresponds to the heteropolar Sb–Se bond vibrations, and the peak at 252 cm^{-1} is attributed to the vibrations of Sb–Sb bonds in (Se_2Sb–$SbSe_2$) s.u. Our result is in agreement with that of Zhang et al. [12] and Ivanova et al. [27]. The exponentially decaying tail near 300 cm^{-1} in the spectrum is due to the Si Raman signal from the substrate and can be subtracted from the spectrum. When compared with the Raman spectrum of antimony trioxide (Sb_2O_3) [28] (as shown in Fig. 12b), the appearance of the two Raman peaks at 147 and 229.5 cm^{-1} indicates that the nanorod contains small amount of oxygen. It was reported in [29] that Sb_2Se_3 nanorods contained Sb_2O_3 when the synthesis temperature was less than 130 °C. Photoluminescence commonly seen in ZnO [30] or Sb_2O_3 [28] 1D nanostructures was attributed to the localized states induced by the presence of oxygen vacancies or defects in the structures. The presence of oxygen in our nanorods may also relate to the observed emission at 700 nm.

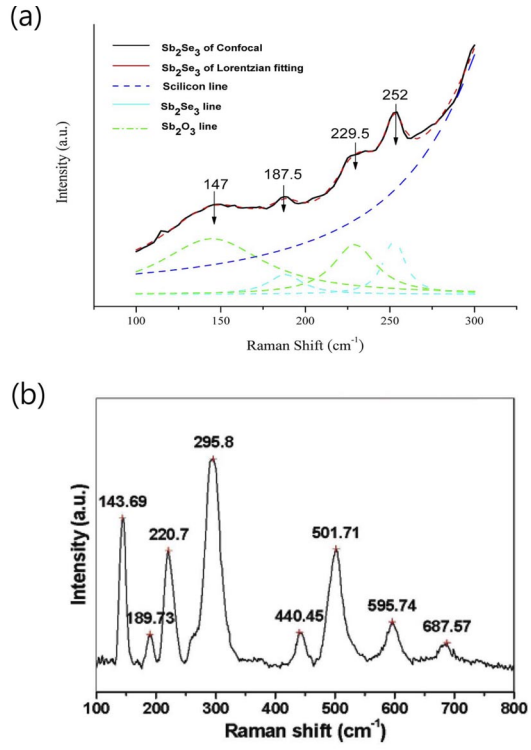

Fig. 12 Raman spectra of (a) a single Sb_2Se_3 nanorod and (b) Sb_2Se_3 nanorod powder.

CONCLUSION

In summary, we demonstrated a solvothermal method for synthesizing the nanocrystalline Sb_2Se_3 rods from a single-source precursor. This simple process is favorable for the future bulk synthesis of other nanomaterials with complex nanostructures and the technological importance. The obtained materials were characterized by XDR, EDS, SEM, TEM, and optical spectrum analysis in detail. By combining a confocal microscope and an E-beam patterned smart substrate, we were able to study the photoluminescence and Raman spectra of nanorods on a single nanostructure basis. In contrast to earlier reports on Sb_2Se_3 nanostructure powder or clusters, the factors arising from size distribution can be ruled out. The observed broad linewidth of luminescence spectra from the single rod can be attributed to the increased number of surface defects, impurities, and dangle bonds attached to the surface as the nanoparticle size is reduced to nanometer scale. The Raman results reveal that Sb_2Se_3 nanorods fabricated at the lower temperature contain a small amount of Sb_2O_3. The luminescence emission deserved additional investigation, which suggests that Sb_2Se_3 nanorods may be very promising in the family of functional semiconductor materials. Our measuring technique might make it possible to investigate the photovoltaic and thermo-electrical properties of a single Sb_2Se_3 nanorod and might find potential applications in the construction of miniaturized optoelectric or thermoelectric nanodevices.

ACKNOWLEDGMENT

This work was supported by the National Science Council of the Republic of China under contract No. NSC 96-2112-M-009-024-MY3 and the MOE ATU program.

REFERENCES

1. N. S. Platakis, H. C. Gatos. *Phys. Status Solidi A* **13**, K1 (1972).
2. J. Black, E. M. Conwell, L. Sigle, C. W. Spencer. *J. Phys. Chem. Solids* **2**, 240 (1957).
3. K. Y. Rajapure, C. D. Lokhande, C. H. Bhosele. *Thin Solid Films* **311**, 114 (1997).
4. V. B. Nascimento, V. E. de Carvalho, R. Paniago, E. A. Soares, L. O. Ladeira, H. D. Pfannes. *J. Electron Spectrosc.* **104**, 99 (1999).
5. K. Y. Rajpure, C. D. Lokhande, C. H. Bhosale. *Mater. Res. Bull*. **34**, 1079 (1999).
6. F. D. Rosi, B. Abeles, R. V. Jensen. *J. Phys. Chem. Solids* **10**, 191 (1959).
7. D. Arivouli, F. D. Gnanam, P. Ramasamy. *J. Mater. Sci. Lett*. **7**, 711 (1988).
8. N. Kh. Abrikosov, V. F. Bankina, L. V. Poretakaya, L. E. Skudnova, E. V. Skudnova. In *Semiconductor II-VI and V-VI Compounds*, A. Tybulewicz (Ed.), p. 186, Plenum, New York (1969).
9. J. Wang, Z. Deng, Y. Li. *Mater. Res. Bull.* **37**, 495 (2002).
10. (a) D. Wang, D. Yu, M. Shao, W. Yu, Y. Qian. *Chem. Lett.* **31**, 1056 (2002); (b) D. Wang, D. Yu, M. Shao, W. Yu, Y. Qian. *J. Cryst. Growth* **253**, 445 (2003).
11. Q. Xie, Z. Liu, M. Shao, L. Kong, W. Yu, Y. Qian. *J. Cryst. Growth* **252**, 570 (2003).
12. Y. Zhang, G. Li, B. Zhang, L. Zhang. *Mater. Lett.* **58**, 2279 (2004).
13. G.-Y. Chen, B. Dneg, G.-B. Cai, T.-K. Zhang, W.-F. Dong, W.-X. Zhang, A.-W. Xu. *J. Phys. Chem. C* **112**, 672 (2008).
14. D. Wang, D. Yu, M. Shao, J. Xing, Y. Qian. *Mater. Chem. Phys*. **82**, 546 (2003).
15. X. Zheng, Y. Xie, L. Zhu, X. Jiang, Y. Jia, W. Song, Y. Sun. *Inorg. Chem*. **41**, 455 (2002).
16. M. Chen, L. Gao. *Mater. Res. Bull.* **40**, 1120 (2005).
17. G. Shen, D. Chen, K. Tang, X. Jiang, Y. Qian. *J. Cryst. Growth* **252**, 350 (2003).
18. S. Xu, W.-B. Zhao, J.-M. Hong, J.-J. Zhu, H.-Y. Chen. *Mater. Lett.* **59**, 319 (2005).
19. H. Cui, H. Liu, J. Wang, X. Li, F. Han, R. I. Baoughton. *J. Solid State. Chem*. **271**, 456 (2004).
20. X. Qiu, C. Burda, R. Fu, L. Pu, H. Chen, J. Zhu. *J. Am. Chem. Soc.* **126**, 16276 (2004).
21. M. V. Kudchadker, R. A. Zingaro, K. J. Irgolic. *Can. J. Chem*. **46**, 1415 (1968).
22. V. Krishnan, R. A. Zingaro. *Inorg. Chem*. **8**, 2337 (1969).
24. Y.-F. Lin, H.-W. Chang, S.-Y. Lu, C. W. Liu. *J. Phys. Chem. C* **111**, 18538 (2007).
24. H.-W. Chang, B. Sarkar, C. W. Liu. *Cryst. Growth Des*. **7**, 2691 (2007).
25. H. Richer, Z. P. Wang, L. Ley. *Solid State Commun*. **39**, 625 (1981).
26. X. Ma, Z. Zhang, X. Wang, S. Wang, F. Xu, Y. Qian. *J. Cryst. Growth* **263**, 491 (2004).
27. Z. G. Ivanova, E. Cernoskova, V. S. Vassilev, S. V. Boycheva. *Mater. Lett*. **57**, 1025 (2003).
28. Z. Deng, F. Tang, D. Chen, X. Meng, L. Cao, B. Zou. *J. Phys. Chem. B* **110**, 18225 (2006).
29 J. Wang, Z. Deng, Y. Li. *Mater. Res. Bull.* **37**, 495 (2002).
30. K. Vanheusden, C. H. Seager, W. L. Warren, D. R. Tallant, J. A. Voigt. *Appl. Phys. Lett.* **68**, 403 (1996).